RSC Advances

ROYAL SOCIETY OF CHEMISTRY

www.rsc.org/advances

Cite this: DOI: 10.1039/c0xx00000x

www.rsc.org/xxxxxx

ARTICLE TYPE

Synthesis and characterization of AgI/Ag hybrid nanocomposite with surface-enhanced Raman scattering performance and photocatalytic activity

Qingli Huang, Shengping Wen, and Xiashi Zhu*

Received (in XXX, XXX) Xth XXXXXXXXX 20XX, Accepted Xth XXXXXXXXX 20XX
DOI: 10.1039/b000000x

In this paper, a multifunctional platform for detection and degradation of prohibited colorants based on AgI/Ag hybrid nanocomposites through a facile wet-chemical route was successfully fabricated. The AgI/Ag hybrid nanocomposites were characterized by X-ray diffraction, field emission scanning electron microscopy (FESEM), high resolution transmission electron microscopy (HRTEM), energy-dispersive spectroscopy (EDS) and UV-vis diffuse reflectance spectra (DRS). The surface-enhanced Raman scattering (SERS) performance and photocatalytic activity of AgI/Ag hybrid nanocomposites were investigated, respectively. The results showed that the AgI/Ag hybrid nanocomposites exhibit good SERS performance for malachite green (MG) and excellent photocatalytic activity of rhodamine B (RB). The proposed method has advantages in terms of providing a simple and rapid method for the sensitive analysis of prohibited additive colorants.

1. Introduction

Surface-enhanced Raman scattering (SERS) has grown to become a very active field of research in several areas of materials and analytical sciences [1-6]. Consider the application of SERS, it is necessary to develop an efficient SERS substrate that not only can possess strong enhancement factors, but also can be reproducible. Furthermore, the SERS substrates become cheaper and easier to be fabricated and handled are also very important for SERS as a generally analytical tool. Compared with other materials, silver has been demonstrated as the most suitable material for SERS studies. Unfortunately, although considerable progress has been made towards improving and optimizing Ag nanostructures for analytical applications [7-13], the poor reproducibility of Ag SERS active nanostructures is still one major problem for practical applications due to its inhomogeneous distribution in particle size. The fabrication of high throughput, low-cost and reproducible SERS platforms with a narrow size distribution is still a challenging task[14].

Recently, the hybrid nanomaterials that comprise two or more different components have attracted much attention for their unique shape- and composition-dependent properties and multiple functionalities, which are not usually achievable in single-component nanomaterials [15-23]. The multiple functionalities and even novel properties make the hybrid nanomaterials achieve applications in diverse areas, such as multimodal catalysis, chemical detection, and optoelectronic applications [15-23]. Among these hybrid nanomaterials, AgI based hybrid nanocomposites have become an active frontier because of their remarkable optical, electrical, and catalytic properties[24-27]. Silver iodide (AgI) is a direct-gap semiconductor that exhibits two distinct phases at room temperature, wurtzite β-AgI with a hexagonal close-packed lattice and zinc-blende γ-AgI with a face-centered cubic (fcc) lattice [28]. There are many literatures reporting AgI based composites and their ionic conductivity, photoluminescence properties and photocatalytic properties [24-27]. However, the literature about the synthesis and multiple functionalities application of AgI/Ag hybrids is relative few[29-34].

In the present work, a facile, rapid, harmless and low-cost wet chemical method was for preparation of AgI/Ag hybrid nanocomposites as multifunctional platform. The structure and morphology of the as-prepared samples were characterized by using X-ray diffraction (XRD), field emission scanning electron microscopy (FESEM), high resolution transmission electron microscopy (HRTEM), energy-dispersive spectroscopy (EDS) and UV-vis diffuse reflectance spectroscopy (DRS). Malachite green (MG) and rhodamine B (RB) were used to investigate the SERS performance and photocatalytic activity of AgI/Ag hybrid nanocomposites, respectively.

2. Experimetal section

2.1. Material and apparatus

All the chemical reagents used in this work, are analytically pure and were used as received without further purification. Deionized water was used throughout the experiment. The phase purity of the products was characterized by X-ray diffraction (XRD, German Bruker AXSD8 ADVANCE X-ray diffractometer) using a X-ray diffractometer with Cu KR radiation (λ=1.5418 Å). Scanning electron microscope (SEM) images were obtained on a Japan Hitachi S-4800 field emission scanning electron microscopy. Transmission electron microscope (TEM) images,

high resolution transmission electron microscopy (HRTEM) images, high angle annular dark field (HAADF) images and elemental mapping images were obtained on an American FEI Tecnai G2 F30 S-TWIN field-emission transmission electron microscopy (operated at 300 kV). The ultraviolet–visible (UV–vis) diffuse reflectance spectra were obtained on a Amercia Varian Cary 5000 spectrophotometer. Raman spectra were measured using a Britain Renishaw Invia Raman spectrometer with a solid-state laser (excitation at 532 nm, 35mW) at room temperature in the range of 1800–400cm^{-1}. Spectra were accumulated 1 scans. The total accumulation time for SERS and Raman measurements was 10 s. The beam diameter was approximately 1 μm on the sample surface.

2.2. Procedures

2.2.1 Synthesis of AgI/Ag hybrid nanocomposites

2.0 mmol of $AgNO_3$ was dissolved in 40 mL of distilled water with magnetic stirring for 10 min., then, 0.05 g diammonium hydrogen citrate ($C_6H_{14}N_2O_7$) was added into the above solution with stirring and a white precipitates were obtained. Finally, 20 mL 0.1 mol L^{-1} ascorbic acid aqueous solution was poured into the above suspension and stirred for 1 h. The powder was then isolated and washed several times with distilled water.

The as-synthesized Ag microspheres were added into 40 mL distilled water, then a certain amount of 0.1 mol L^{-1} KI (0, 0.2mL, 0.5mL, 1mL, 2mL) aqueous solution was added into the above solution. Afterwards, the same amount of $AgNO_3$ (0, 0.2mL, 0.5mL, 1mL, 2mL) was added into the above solution. The resulting mixture was maintained at room temperature for 1 h. Vigorous stirring was employed throughout the synthesis. For the fast sedimentation rate of AgI/Ag hybrids, the products were isolated by pouring the solution after natural sedimentation for 5 min and washed several times with distilled water and ethanol by the same natural sedimentation methods. Then the products were filtered using filter paper. Finally, the products were dried in vacuum at 60℃ for 3 h. The final products were denoted as S_0, $S_{0.2}$, $S_{0.5}$, S_1 and S_2 respectively.

2.2.2. Characterization

The as-prepared AgI/Ag hybrid nanocomposites were characterized by XRD, FESEM, HRTEM, EDS, UV-vis, and Raman spectrometer.

2.2.3 SERS

Malachite green (MG) were used as Raman probe for the SERS measurements. Different concentrations of MG aqueous solutions were prepared. For preparation of SERS substrates, the as-prepared products were immersed in different concentration of dilute solutions of MG for 12 h, respectively. Then these sample solutions were carefully dropped on specially cleaned glass slides and dried in air. Finally, the SERS of the samples were measured using a Britain Renishaw Invia Raman spectrometer with a solid-state laser (excitation at 532 nm, 35mW) at room temperature in the range of 1800-400cm^{-1}.

2.2.4 Photocatalytic properties

The photocatalytic activity of the samples was evaluated by photodegradation of RB under visible light (532nm Xe lamp). AgI/Ag hybrids (150 mg) were dispersed into 30 mL RB aqueous solution (10^{-5} mol·L^{-1}) and magnetically stirred in the dark for 30min to establish adsorption equilibrium. The concentration of RB was analyzed by UV-vis spectroscopy.

3. Results and Discussion

3.1 Characterization of AgI/Ag hybrid nanocomposites

3.1.1 XRD patterns of AgI/Ag hybrid nanocomposites

The XRD patterns of the products obtained before and after modifying different amount of AgI nanopartiles (NPs) are shown in Fig.1. Comparison with the data of JCPDS card files no.4-783, all diffractions of the product prepared before modifying AgI NPs (S_0) can be indexed to cubic Ag (Fig. 1a), new peaks centered at ~22.2°, 23.6°, 25.3°, 39.2° and 46.2° appeared, which could be indexed as hexagonal AgI (JCPDS no.83-2044) after modifying AgI NPs (Fig. 1b-e). Furthermore, it could be clearly seen that the peaks of AgI crystals were significantly enhanced with the amount of AgI increase.

<Fig. 1>

3.1.2 Electron microscopy characterization of AgI/Ag hybrid nanocomposites

The morphologies of the Ag NPs before and after modifying AgI were observed by FESEM. Fig.2a exhibited a representative FESEM image of pure Ag microspheres (S_0), it comprised abundant microspheres with the diameter of 2~3 μm. The surfaces of microspheres were clean. For AgI/Ag hybrid nanocomposites, FESEM observations showed that some NPs strew on the surface of microspheres (Fig.2 b-e) while the size of Ag microspheres does not change obviously. The size and the amount of AgI NPs were increased with amount of the reactants (KI and $AgNO_3$). By adding 0.2mL reactants (KI and $AgNO_3$), there are few nanoparticles on the surface of the microspheres (Fig. 2b). The diameter of these nanoparticles is only ca 40 nm. When the amount of the reactants (KI and $AgNO_3$) is increased to 0.5mL, AgI NPs become more and the size of these nanopartices is increased to about 50 nm (Fig. 2c). Further increasing the volume of the reactants to 1 mL and 2mL (Fig.2 d and e), AgI NPs further become more and the size of the particles increased to about 70 nm and 80 nm, respectively (Fig.2 d and e). And, the NPs on the surface of microspheres began aggregated. It can be conclude that the volume of the reactants play a key role in the preparation of AgI/Ag hybrid nanocomposites.

<Fig. 2>

The high angle annular dark field (HAADF) and energy-dispersive spectroscopy elemental mapping images of $S_{0.5}$ in Fig.3a-c revealed the distribution of I^- on the surface of Ag microspheres, which is homogeneous. TEM and HRTEM analysis were also performed to confirm the structures of the $S_{0.5}$. The TEM image in Fig.3d further confirmed their spherical structures doped with many nanoparticles. The interplanar spacing of 0.24 nm corresponds to the (100) plane of Ag, while 0.35 nm corresponds to the (101) plane of AgI. A continuity of lattice fringes between the interface of Ag and AgI indicates the formation of AgI/Ag heterojunction (Fig.3 e).

<Fig. 3>

3.2 Surface-enhanced Raman scattering performance and photocatalytic activity

3.2.1 SERS

Malachite green (MG) is still being used as a fungicide and antiseptic in many countries due to its low cost, availability, and efficacy. The abuse of MG in the aquaculture has become a great

concern, because it causes potential genotoxicity and carcinogenicity to living organisms. In this work, different concentrations of MG were employed as Raman probes for the SERS efficiency of the as-prepared AgI/Ag hybrids. Despite at the expense of the part of enhancement effect, the as-prepared AgI/Ag hybrid nanocomposite ($S_{0.5}$) is suitable as SERS substrate for its better reproducibility (Fig. 4) [35]. Well defined Raman signals of MG were demonstrated in Fig. 4. SERS spectra of MG acquired with $S_{0.5}$ as SERS substrates are consistent with that of their corresponding solid powers (Fig. 5 curve e) [36]. The peaks at 447, 1179, 1368 and 1621 cm^{-1} were caused by out of-plane modes of phenyl-C-phenyl, in-plane modes of ring C-H bending, N-phenyl stretching, ring C-C stretching, respectively. The medium bands at 803, 1220 and 1400 cm^{-1} were attributed to out-of-plane modes of ring C-H, C-H rocking and N-phenyl stretching, respectively. C-N-C bending was observed at 537 cm^{-1}, and C-H out of-plane bending at 913 cm^{-1}.

<Fig. 4>

The spectral intensities and resolutions were decreased by diluting the concentration of the target molecule (MG) (Fig. 5 curve a-d). It is found that additional MG peaks still appeared at the concentration of 10^{-6} mol L^{-1} (Fig. 5 curve c). We estimated the average enhancement factor (EF) calculated according to the following formula [37]

$$EF = \frac{I_{SERS} / I_{Raman}}{N_{surface} / N_{bulk}} \quad (1)$$

where I_{SERS} stands for the intensities of the vibrational mode in the SERS spectra and I_{Raman} stands for the same vibrational mode in the normal Raman spectra. These data can be directly obtained from the experiment. N_{bulk} and $N_{surface}$ are the number of MG molecules illuminated by the laser focus spot under normal Raman and SERS conditions, respectively. Here, the 1621 cm^{-1} band having the highest peak intensity was selected for such a calculation, which can be assigned to the aromatic stretching vibration. They were calculated on the basis of the estimation of the concentration of the surface species or bulk sample and the corresponding sampling area. $N_{surface}$ can be obtained according to the reported method [36]. In Fig. 5, we obtained that the I_{SERS} and I_{Raman} 9757 and 673 counts at the Raman band of 1621 cm^{-1}, respectively. In the normal Raman spectrum, the neat solid sample was used, whereas the dissolved concentration was 10^{-4} mol·L^{-1} in the SERS spectrum. The volumes of the irradiated laser spots in the Raman and SERS experiments were identical. Assuming the density of 1 g/cm^{-3} for the solid MG, the enhancement factor may be estimated as $(9757) \times (10^5) \times 1/(673) \times (1/365) \times (10^3) = 5.29 \times 10^5$.

<Fig. 5>

The reproducibility of the substrate is an important factor for SERS detection. the SERS spectra of MG were collected from 6 random points on different as-prepared AgI/Ag hybrids nanocomposites (S_0, $S_{0.2}$, $S_{0.5}$, S_1 and S_2). Fig.6 depicted the SERS signal of MG in a intensity-laser spot at 1621 cm^{-1}. The relative standard deviation (RSD) of SERS intensity for 6 different sites on AgI/Ag hybrid nanocomposites (S_0, $S_{0.2}$, $S_{0.5}$, S_1 and S_2) are calculated. The order of RSD was $RSD(S_0)$ =48.1%>>$RSD(S_{0.2})$=29.3%> $RSD(S_2)$=28.4%> $RSD(S_1)$=19.4%> $RSD(S_{0.5})$ =8.5%, it is clearly concluded that SERS substrate $S_{0.5}$ showed the best reproducibility. In order to investigated the uniformity of SERS signals of the as-prepared hybrids, SERS mapping was also carried out. The green spots on the SERS mappings indicates the uniformity of SERS signals of MG on $S_{0.5}$ (Inset image in Fig. 6). A reasonable mechanism for the superior SERS reproducibility may be attributed to the uniform distribution of AgI NPs on the surface of Ag microspheres.

<Fig. 6>

3.2.2 Photocatalytic activity

As is known to all, the photocatalytic activity of Ag/AgX (Cl, Br, I) are related to their optical properties. The UV-vis diffuse reflectance spectra of the as-prepared products (S_0, $S_{0.2}$, $S_{0.5}$, S_1 and S_2) were investigated. Fig. 7 displays the UV-visible diffuse reflectance spectra of Ag (S_0) and the as-prepared AgI/Ag hybrid nanocomposites (S_0, $S_{0.2}$, $S_{0.5}$, S_1 and S_2). It can be clearly seen that absorption at 319 nm and 370 nm were found, which are associated with the optical band gap and the surface plasma resonance of pure Ag microspheres, respectively (Fig 7a). For AgI/Ag hybrid nanocomposites, a new absorbance peak centered at 427 nm was observed (Fig 7b-e), which is attributed to the characteristic band of β-AgI (wurtzite), induced by the forbidden transition ($4d^{10}$ to $4d^9 5s^1$) in the Ag ion [34]. With increasing the volume of the reactants (Fig 7b-e), there is a slight gradual enhancement of the absorption peak centered at 427 nm, suggesting the increasing amount of AgI nanoparticles. At the same time, the absorption centered at 427 nm appears red-shift. When the particle size increases, higher order surface modes may become dominant. It may induce a shift of the absorption maximum toward lower energies, a broadening of the absorption band [34]. This result is consistent with the former discovery that the amount and the size of AgI nanoparticles on the surface of Ag increases with increasing the volume of the reactants.

<Fig. 7>

RB was employed as a probe to test photocatalytic activity of AgI/Ag hybrid nanocomposites under visible light irradiation, the photodegradation process was monitored by both UV-visible spectroscopy and SERS spectra. The evolution of the absorption spectra of RB under visible light irradiation was shown in Fig. 8a. The characteristic absorption peaks of RB gradually weakened and almost disappeared from the absorption spectra within 60 min, which indicated degradation of RB. Similarly, SERS spectra were adopted to track the process of photocatalytic degradation of RB (Fig.8b). It could be seen that the SERS peaks of RB gradually weakened within 60 min. As a result, UV-visible spectroscopy and SERS spectra both could be used to effectively monitor the photodegradation process of RB based on the as-prepared AgI/Ag hybrid nanocomposites ($S_{0.5}$) and the AgI/Ag exhibited high photocatalytic activity for RB and could be used as photocatalyst for degradation of organic dyes.

<Fig. 8>

The photocatalytic activities of AgX/Ag (Cl, Br) hybrids were extensively studied by many groups [15-23]. In this work, the as-prepared AgX/Ag hybrid nanocomposites were prepared under the same condition. Fig. 9 plotted the RB concentration ratio(C/C_o) as a function of irradiation time over AgI/Ag hybrids, AgCl/Ag hybrids, AgBr/Ag hybrids and pure Ag prepared. It could be seen from Fig.9 that AgI/Ag hybrids showed the highest conversion. RB conversion over AgI/Ag hybrids, AgCl/Ag

hybrids, AgBr/Ag hybrids and pure Ag was 93%, 76%, 48% and 6% respectively after 1h of visible light irradiation.

<Fig. 9>

In order to illustrate the reason for the higher RB conversion of AgI/Ag hybrids, the morphologies of the corresponding AgX/Ag (Cl, Br) hybrids were also investigated, which were shown in EIS (Fig.10). Obviously, AgCl and AgBr particles are hard to deposit on the surface of Ag microspheres, which led to the formation of simple mixture of AgX (Cl, Br) and Ag microsheres. Therefore, the formation of heterojunction structure and the uniform deposition of AgI nanoparticles in the as-synthesized AgI/Ag composites enlarge the interface between the AgI and Ag, which accelerates the separation and migration of electrons and holes and leads to the high photocatalytic activity. In the AgI/Ag hybrids system, photons from the visible light irradiation could be absorbed by AgI and Ag^0, and the photogenerated electrons and holes were produced. Synergy effect between Ag microspheres and the polarization field provided by the AgI nanoparticles facilitates electron-hole separation and interfacial charge transfer. As a result, electrons accumulate on the surface of the Ag microspheres to reduce desired species at the Ag/solution interfaces, while the left over holes diffuse into the AgI to oxidize I^- ions to I atoms, which are very reactive for oxidizing species in the surround solutions. The I atoms will be reduced back to I^- ions. As a result, redox reactions of organic pollutants can be driven by visible light[24,27,29,30].

<Fig. 10>

4. Conclusions

AgI/Ag hybrid nanocomposites have been successfully synthesized by precipitation of $AgNO_3$ and KI on the surface of Ag microspheres. The products were characterized by XRD, FESEM, HRTEM and UV–vis. It showed that AgI nanoparticles strew on the surface of Ag microspheres and the formation of heterojunction structure between Ag and AgI and which exhibit good SERS performance for malachite green (MG) and photocatalytic activity of rhodamine B (RB).

Notes

College of Chemistry & Chemical Engineering, Yangzhou University, Yangzhou 225009, China
Corresponding author. Tel.: +86 514 7975244; fax: +86 514 7975244.
E-mail addresses: xszhu@yzu.edu.cn, zhuxiashi@sina.com (X. Zhu).

ACKNOWLEDGEMENTS

The authors acknowledge the financial support from the National Natural Science Foundation of China (21375117, 21155001), Technology Invention Foundation of Yangzhou University (2013CXJ087) and excellent PhD dissertation Foundation of Yangzhou University.

References:

1. J. Perumal, K. V. Kong, U. S. Dinish, R. M. Bakker,Malini Olivo, *RSC Adv*., **2014**, *4*, 12995–13000
2. M.D. Porter, R.J. Lipert, L.M. Siperko, G. Wang, R. Narayanana, *Chem. Soc. Rev.* **2008,** *37,* 1001–1011.
3. S. Kundu, U. Nithiyanantham, *RSC Adv.*, **2013**, *3*, 25278–25290.
4. X.S. Shen, G.Z. Wang, X. Hong,W. Zhu, *Phys. Chem. Chem. Phys.* **2009,** *11,* 7450–7454.
5. M. Futamata, *Faraday Discuss.* **2006,** *132,* 45–61.
6. X. Gong, Y. Bao, C. Qiu, C.Y. Jiang, *Chem. Commun.*, **2012**, *48*, 7003-7018.
7. M.Z. Si, Y.P. Kang, R.M. Liu，*Appl. Surf. Sci.* **2012**, *258*, 5533– 5537
8. S.E. Skrabalak, L. Au, X. D. Li, Y.N. Xia, *Nature Protocols* **2007**, *2*, 2182-2190.
9. Q. Zhang, C.M. Cobley, L. Au, M. McKiernan, A. Schwartz, L.P. Wen, J.Y. Chen, Y.N. Xia, *ACS Appl. Mater. Interf.* **2009**, *1*, 2044-2048.
10. D.A. Clayton, T. E. McPherson, S.L. Pan, M.Y. Chen,D.A. Dixon, D.H. Hu, *Phys. Chem. Chem. Phys.,* **2013**, *15*, 850--859
11. Y.Y. Liu, Y.X. Zhang, H.L. Ding, S.C. Xu, M. Li, F.Y. Kong,Y.Y. Luo, G.H. Li, J. Mater. Chem. A, **2013**, *1*, 3362–3371.
12. T. Liu, D.S. Li, D.R. Yang, M.H. Jiang, *Langmuir* **2011**, *27*, 6211–6217.
13. M.F. Zhang, A.W. Zhao, H.H. Sun, H.Y. Guo, D.P. Wang, D. Li, Z.B. Gan, W.Y. Tao, *J. Mater. Chem.* **2011**, *21*, 18817-18824.
14. J.F. Betz, W.W. Yu, Y. Cheng, I.M. White, G.W. Rubloff, *Chem. Chem. Phys.,* **2014**, *16*, 2224–2239.
15. L. Tzounis, R. Contreras-Caceres, L. Schellkopf, D. Jehnichen, D. Fischer, C.Z. Cai, P. Uhlmann, M. Stamm，*RSC Adv.* **2014**, *4*, 17846–17855.
16. Y.M. Dong, C.Y. Feng, P.P. Jiang, G.L. Wang, K. Li, H.Y. Miao, *RSC Adv.* **2014**, *4*, 7340–7346.
17. H. Xu, Y.G. Xu, H.M. Li, J.X. Xia, J. Xiong, S. Yin, C.J. Huang, H.L. Wan, *Dalton Trans.* **2012**, *41*, 3387–3394.
18. L.X. Chen,N. Qi, X.K. Wang, L. Chen, H.Y. You ,J.H. Li, *RSC Adv.*, **2014**, *4*, 15055–15060.
19. P. Wang, B.B. Huang, X.Y. Qin, X.Y. Zhang, Y. Dai, J.Y. Wei, M.H. Whangbo, *Angew. Chem. Int. Ed.* **2008**, **47**, 7931–7933.
20. C.H. An, R.P. Wang, S.T. Wang, X.Y. Zhang, *J. Mater. Chem.* **2011**, *21*, 11532–11536.
21. H. Xu, H.M. Li, J.X. Xia, S. Yin, Z.J. Luo, L. Liu, L. Xu, *ACS Appl. Mater. Interf.* **2011**, *3*, 22–29.
22. L. Han, P. Wang, C.Z. Zhu, Y.M. Zhai, S.J. Dong, *Nanoscale* **2011**, *3*, 2931–2935.
23. P. Wang, B.B. Huang, X.Y. Zhang, X.Y. Qin, H. Jin, Y. Dai, Z.Y. Wang, J.Y. Wei, J. Zhan, S.Y. Wang, J.P. Wang, M.H. Wangbo, *Chem. Eur. J.* **2009**, *15*, 1821–1824.
24. Y.P. Bi, S.X. Ouyang, J.Y. Cao, J.H. Ye, *Phys. Chem. Chem. Phys.* **2011**, *13*, 10071–10075.
25. K. Vignesh, A. Suganthi, M. Rajarajan, S.A. Sara, *Powder Technol.*, **2012**, *224*, 331–337.
26. H.F. Cheng, W.J. Wang, B.B. Huang, Z.Y. Wang, J. Zhan, X.Y. Qin, X.Y. Zhang, Y. Dai, *J. Mater. Chem. A***, 2013**, *1*, 7131–7136.
27. C.H. An, W. Jiang, J.Z. Wang, S.T. Wang, Z.H. Ma, Y.P. Li, *Dalton Trans.*, **2013**, *42*, 8796–8801.
28. O. Ohtaka, H. Takebe, A. Yoshiasa, H. Fukui and Y. Katayam, *Solid State Commun.* **2002**, *123*, 213–216
29. H.G. Yu, Li Liu, X.F. Wang, P. Wang, J.G. Yu, Y.H. Wang, *Dalton Trans.*, **2012**, *41*, 10405–10411.
30. C.H. An, J.Z. Wang, J.X. Liu, S.T. Wang, Q.H. Zhang, RSC Adv., **2014**, *4*, 2409–2413.
31. H. L. Lin, J. Cao, B. D. Luo, B. Y. Xu, S. F. Chen, *Catal. Commun.*, **2012**, *21*, 91–95.
32. M.C. Long, W.M. Cai, *Nanoscale***, 2014**, *6*, 7730–7742
33. C. Hu, T.W. Peng, X.X. Hu, Y.L. Nie, X.F. Zhou, J.H. Qu, H. He, *J. Am. Chem. Soc.* **2010**, *132*, 857–862.
34. C. Yang, Y.T. Xie, M.M. F. Yuen, X.M. Xiong, C. P. Wong, *Phys. Chem. Chem. Phys.,* **2010**, *12*, 14459–14461
35. L. Rodriguez-Lorenzo, L. Fabris, R. A. Alvarez-Puebla, *Anal. Chim. Acta* **2012**, *745*, 10– 23.
36. G. H.Gu, J.S. Suh, *J. Raman Spectrosc.* **2010**, *41*, 624–627.
37. D.K. Singh, E.O. Ganbold, E. M. Cho, K.H. Cho, D. Kim, J. Choo, S, Kim, C. M. Lee, S.I. Yang, S.W. Joo, *J. Hazard. Mater.* **2014**, *265*, 89– 95.

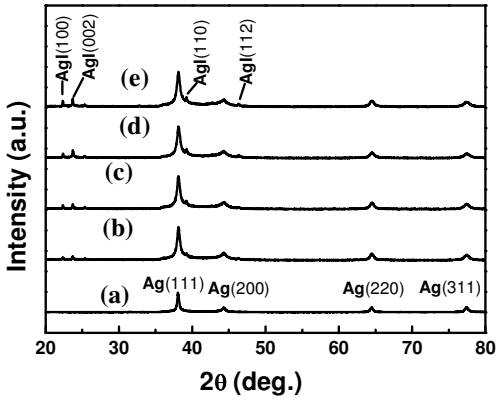

Fig.. 1. XRD patterns of AgI/Ag hybrid nanocomposites synthesized with a different amount of the reactants (KI and $AgNO_3$) : (a) 0 mL, (b) 0.2 mL, (c) 0.5 mL (d) 1 mL and (e) 2mL.

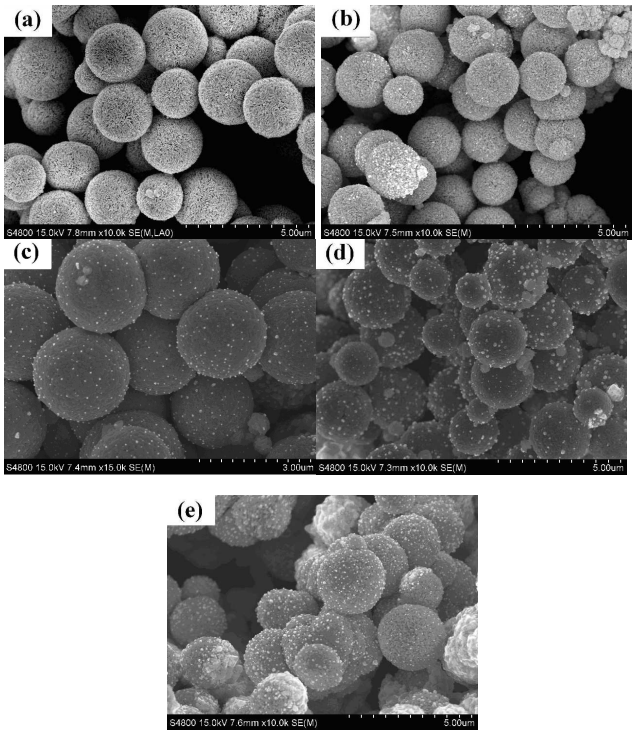

Fig. 2. FESEM images of AgI/Ag hybrid nanocomposites synthesized with different amount of the reactants (KI and $AgNO_3$): (a) 0 mL, (b) 0.2 mL, (c) 0.5 mL, (d) 1 mL and (e) 2mL.

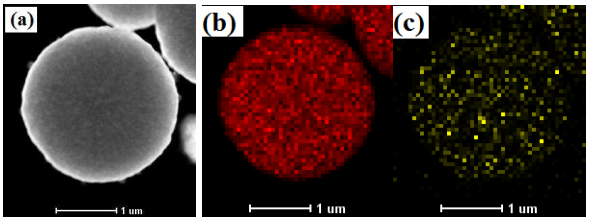

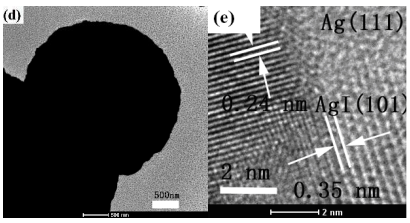

Fig. 3. HAADF, elemental mapping, TEM and HRTEM images of the as-prepared samples $S_{0.5}$ (a) HAADF image (b) Ag elemental mapping (c) I elemental mapping (d) TEM image and (e) HRTEM images.

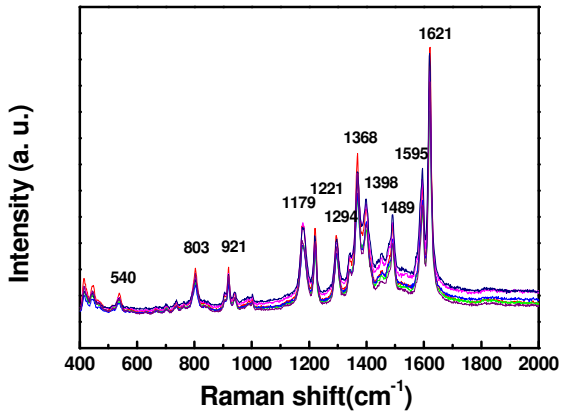

Fig. 4. Reproducible SERS spectra of 10^{-4} mol·L^{-1} malachite green dropped on the as-prepared hybrids $S_{0.5}$.

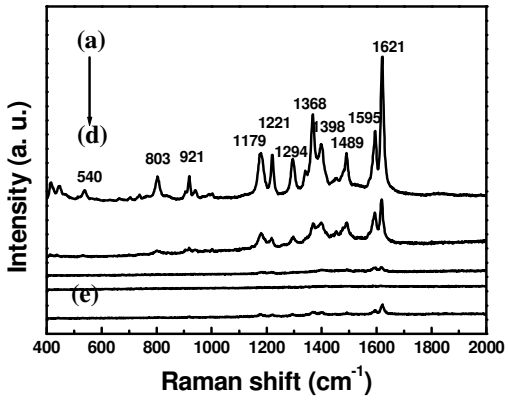

Fig.5. SERS spectra of different concentration of malachite green dropped on the as-prepared hybrids $S_{0.5}$ (a) 10^{-4} mol·L^{-1}, (b) 10^{-5} mol·L^{-1}, (c) 10^{-6} mol·L^{-1}, (d) 10^{-7} mol·L^{-1} and (e) Raman spectrum of pure malachite green.

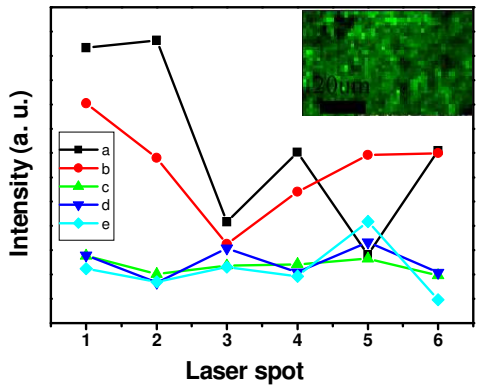

Fig.6. The relationship between the SERS intensity of malachite green (10^{-4} mol·L^{-1}) at different plot at 1621 cm^{-1} of different samples synthesized with different amount of the reactants (KI and $AgNO_3$) : (a) 0 mL(S_0), (b) 0.2 mL($S_{0.2}$), (c) 0.5 mL($S_{0.5}$), (d) 1 mL(S_1) and (e) 2mL(S_2) (the inset image is SERS intensity maps of malachite green (10^{-4} mol·L^{-1}) at 1621 cm^{-1} composed of 1500 spectra using $S_{0.5}$ as SERS substrate).

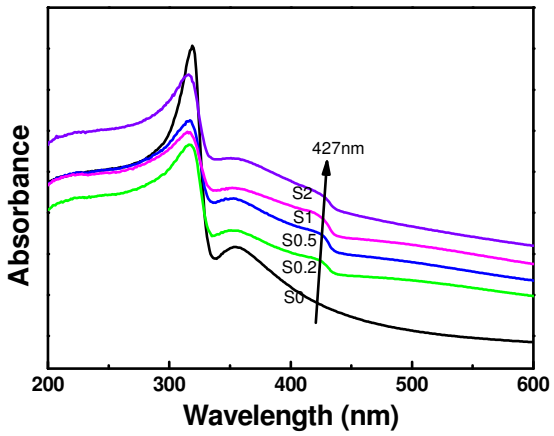

Fig.7. UV–vis diffuse reflectance spectra for the samples synthesized with different amount of the reactants (KI and $AgNO_3$).

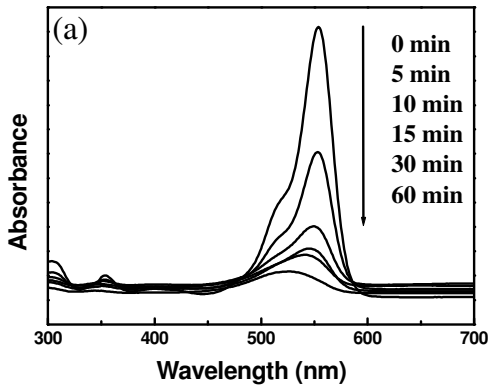

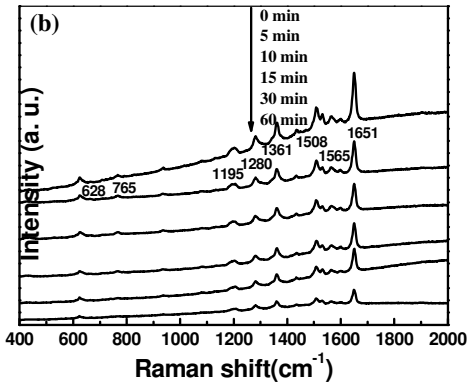

Fig.8. (a) The UV-visible and (b) SERS spectra of RB dye under visible light irradiation using AgI/Ag hybrids ($S_{0.5}$) in 1 h

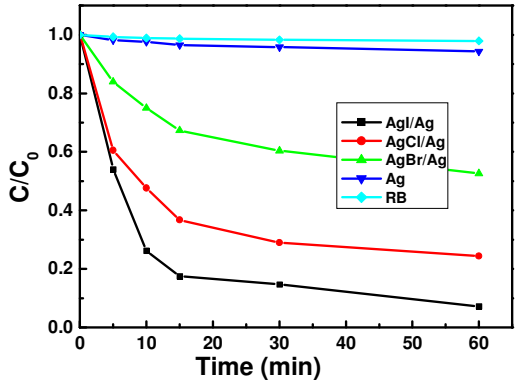

Fig.9. Photocatalytic degradation of RB with various samples under visible light irradiation in 1 h.

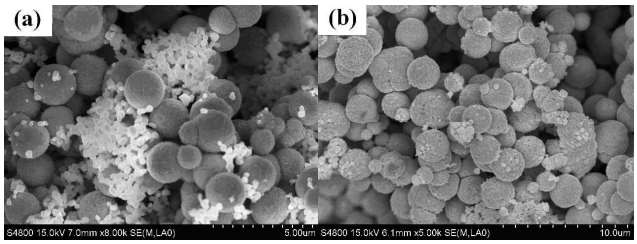

Fig. 10. FESEM images of the as-prepared sample (a) AgCl/Ag hybrids and (b) AgBr/Ag hybrids